Original article

Designing chitosan based magnetic beads with conocarpus waste-derived biochar for efficient sulfathiazole removal from contaminated water

Mohammad I. Al-Wabel [a,*], Munir Ahmad [a], Adel R.A. Usman [a,b], Abdullah S.F. Al-Farraj [a]

[a] Soil Sciences Department, College of Food & Agricultural Sciences, King Saud University, P.O. Box 2460, Riyadh 11451, Saudi Arabia
[b] Department of Soils and Water, Faculty of Agriculture, Assiut University, Assiut 71526, Egypt

A B S T R A C T

The development of a simple method to synthesize highly efficient and stable magnetic microsphere beads for sulfathiazole (STZ) removal from contaminated aqueous media was demonstrated in this study. Conocarpus (Conocarpus erectus L.) tree waste (CW) derived biochar (BC) was modified to fabricate chitosan-BC (CBC) and magnetic CBC (CBC-Fe) microsphere beads. Proximate, chemical, and structural properties of the produced adsorbents were investigated. Kinetics, equilibrium, and pH adsorption batch trials were conducted to evaluate the effectiveness of the synthesized adsorbents for STZ removal. All adsorbents exhibited the highest STZ adsorption at pH 5.0. STZ adsorption kinetics data was best emulated using pseudo-second order and Elovich models. The equilibrium adsorption data was best emulated using Langmuir, Freundlich, Redlich–Peterson, and Temkin models. CBC-Fe demonstrated the highest Elovich, pseudo-second order, and power function rate constants, as well as the highest apparent diffusion rate constant. Additionally, Langmuir isotherm predicted maximum adsorption capacity was the highest for CBC-Fe (98.67 mg g^{-1}), followed by CBC (56.54 mg g^{-1}) and BC (48.63 mg g^{-1}). CBC-Fe and CBC removed 74.5%–108.8% and 16.2%–25.6% more STZ, respectively, than that of pristine BC. π-π electron-donor–acceptor interactions and Lewis acid-base reactions were the main mechanisms for STZ removal; however, intraparticle diffusion and H-bonding further contributed in the adsorption process. The higher efficiency of CBC-Fe for STZ adsorption could be due to its magnetic properties as well as stronger and conducting microsphere beads, which degraded the STZ molecules through generation of HO$^\bullet$ radicals.

1. Introduction

Antibiotics are natural or synthetic chemical agents commonly used to suppress bacterial and parasitic diseases in human and animals. Additionally, antibiotics are used to improve livestock health. It is estimated that the global antibiotic consumption has crossed $63,151 \pm 1,560$ tons in 2010 and may reach to $105,596 \pm 3,605$ tons by 2030 (Van Boeckel et al., 2015). Incomplete metabolism results in excretion of antibiotics from animal via urine and feces. This cre-ates a serious problem for the surrounding environment, water resources, and human habitant in vicinity of the farms. Direct disposal of dry and wet animal effluents along with partially decomposed antibiotics are polluting the fresh and wastewater resources in the vicinity of livestock yards. Consequently, this increases the production and accumulation of antibiotic resistance bacteria (ARB) and antibiotic resistance genes (Wang and Chen, 2020; Wang et al., 2020). In a study conducted to assess potential contamination of antibiotics in water, Huang et al. (2011) found that antibiotic concentrations in untreated wastewater ranged from 3.9 to 27,000 ng L^{-1}. In Saudi Arabia, use of antibiotics in livestock production has become a vital public health concern due to microbial resistance. Enormous use of antibiotics in livestock and poultry farming has resulted in ARB growth and antibiotic residues in meat and milk products. Al-Nazawi (2006) collected milk samples from the Al-Hassa region of Saudi Arabia and found that 9.2% of the milk samples contained antibiotic residues, with 17.1% of these same

* Corresponding author.
E-mail address: malwabel@ksu.edu.sa (M.I. Al-Wabel).

Peer review under responsibility of King Saud University.

milk samples showing production and growth of antibiotic resistant *Staphylococcus aureus* bacteria. In a review study, Al-Mogbel et al. (2015) found that the maximum allowable limit of tetracycline residues in chicken eggs and food borne ARB was exceeded due to misuse of antibiotics in poultry and livestock industries.

Sulfathiazole (STZ), a member of sulfonamide family, is one of the most significant and important antibiotics due to its massive consumption in the fields of medicine, animal husbandry, and poultry production (Awad et al., 2014). Previous studies have reported potential toxicity of STZ in fresh and wastewater resources, sewage treatment plants, aquatic environments and terrestrial ecosystems (Kim and Carlson, 2007; Choi et al., 2008). STZ may enter into the natural system through different pathways including medical waste from expired products, poorly managed wastewater treatment plants, dung and urine from grazing animals, seepage from agricultural waste, and direct disposal of farmyard waste to nearby land and water bodies (Wang et al., 2019). STZ is water soluble because it is a weak acid. Thus, it is likely to run-off into surface water or seep into ground water when released in the environment. Additionally, the toxic effects of STZ on the environment may be compounded due to the presence of other compounds, such as pesticides (Boxall et al., 2003). Dumping of farmyard manure and poultry waste containing partially adsorbed residues of consumed STZ into soil may deteriorate the environment. Thus, STZ residues are characterized as potential organic pollutants that require immediate action to be removed from ecosystem.

Many techniques including biological processing, electrochemical treatment, ozonation, membrane filtration, activated carbon, and advanced oxidation have been employed to mitigate antibiotic contamination in wastewater (Liu et al., 2020; Wang and Zhuan, 2020; Wang and Wang, 2018). Most of these techniques are costly, less efficient, and generate by-products which may cause secondary pollution. These negative factors limit the use of these technologies for antibiotics removal. Adsorption is a widely accepted technology due to its simple design, easy implementation, lower operation costs, and higher efficacy (Liu et al., 2020). However, the efficiency of an adsorption process depends on the type of adsorbent and adsorbate as well as conditions and composition of the medium. Until recently, a variety of low cost adsorbents have been developed and used for antibiotics removal. These include saw dust (Bajpai et al., 2012), date palm leaflets (El-Shafey et al., 2012), corn bracts (Yu et al., 2017) and biochars (Zheng et al., 2013; Ahmad et al., 2019a and b).

Among these adsorbents, biochar, has been globally endorsed as an innovative adsorbent for the removal of a range of environmental pollutants (Lehmann, 2007; Wang and Wang, 2019). Biochar is a solid by-product of organic waste combustion from a controlled oxygen supply that make biochar a promising adsorbent for a variety of pollutants due to its variety of surface functional groups, spongy structure, high specific surface area, and net negative surface charge. However, its heterogeneous nature, high pH and negatively charged surface make it an inconsistent adsorbent (Yao et al., 2013). To address this problem, biochar needs to be activated and modified by certain physical, mechanical, and chemical processes to overcome these restraints and to improve its efficiency as an adsorbent.

Biochar has been engineered with foreign materials to induce desirable functional groups, enhance specific surface areas, and escalate its recalcitrance potential. Biochar engineering has investigated a range of foreign materials such as zeolite, silica, metal oxides, and polymers to improve its adsorption efficiency (Ahmad et al., 2018a; Rafique et al., 2020). For instance, Chen et al. (2019) has reported that addition of –OH functional groups to $FeCl_3 \cdot 6H_2O$-loaded corn husks derived biochar resulted in higher adsorption of levofloxacin and tetracycline due to bidentate complexation and hydrogen bonding. Peng et al. (2014) demonstrated higher adsorption (95.86 mg g^{-1}) of tetracycline by using biochar modified with iron oxide. Chitosan has been investigated as an inexpensive, environment friendly and biodegradable adsorbent with excellent adsorption capacity for a range of pollutants (Wang and Zhuang, 2017; Mututuvari and Tran, 2014). A novel iron imprinted chitosan-Fe^{III} composite adsorbent showed excellent adsorption capacity for simultaneous removal of tetracycline and cadmium in wastewater (Chen et al., 2017). However, the effectiveness of chitosan-biochar-iron microsphere beads for STZ removal from contaminated aqueous media has yet to be explored. Therefore, in this study, conocarpus (*Conocarpus erectus* L.) tree waste-derived biochar was produced and modified to synthesize chitosan-biochar and magnetic chitosan-biochar microsphere beads. The produced adsorptive materials were successfully employed for STZ removal from contaminated water through the pH, kinetics, and equilibrium adsorption batch trials. Further, the efficacy of the synthesized adsorptive materials and adsorption processes were explored by using kinetics and isotherm models.

2. Materials and methods

2.1. Biochar and magnetic biochar production

Conocarpus (*Conocarpus erectus* L.) tree waste, including leaves and small branches, was collected from Riyadh province, Saudi Arabia. After washing with tap water, the collected waste was air-dried. The dried and crushed conocarpus waste (CW) was pyrolyzed in electrical furnace at 400 °C for 180 min. The pyrolysis was conducted under limited oxygen supply with pyrolysis temperature of 5 °C min^{-1}. After completion of the pyrolysis, the furnace was cooled and the obtained charred material was collected, washed with deionized water, and dried at 65 °C in an oven. The dried biochar was then ground into a powder for 30 min using a ball-mill at 650 rpm and labeled as BC.

To synthesize the magnetic biochar, 10 g of BC was suspended in 100 mL of deionized water and then stirred for 120 min to produce a homogenized suspension. Next, a 500 mL solution containing mixture of $FeCl_3 \cdot 6H_2O$ (10 g) and $FeSO_4 \cdot 7H_2O$ (5.55 g) was added to the BC suspension. Then, the mixture was stirred for another 120 min for complete homogenization. This mixture was poured into an air-tight container and hydrolyzed for 120 min at 180 °C. Finally, the hydrolyzed material was collected, washed several times with deionized water and ethanol, and dried at 65 °C.

2.2. Fabrication of microsphere beads

To synthesize the beads, 2.0 mL of acetic acid was mixed with 98 mL of deionized water. 2.0 g of chitosan was dissolved in this solution. Then, 4.0 g of either BC or magnetic BC was added to the acetic acid-chitosan solution and stirred for 180 min to prepare a homogenous suspension. Next, this suspension was drop-wise added to a 1.2% solution of NaOH by using a syringe to form beads of uniform particle size. The produced spherical beads were allowed to float in the solution overnight. The following day, beads were collected and washed with deionized water, and heated in 500 mL deionized water at 60 °C for 120 min under continuous stirring. Finally, the beads were allowed to float in deionized water for 240 min, and then separated. After washing with deionized water, the beads were dried at 60 °C in an oven. Hereafter, chitosan-biochar beads were named as CBC and magnetic chitosan-biochar beads as CBC-Fe.

2.3. Characterization of adsorbents

Chemical, surface, and structural properties of the materials were investigated. Proximate analyses such as ash and moisture contents as well as volatile and fixed matter were analyzed using ASTM D1762-84 standard methods (ASTM, 1989). A 1:10 suspension of adsorbent to deionized water was used to analyze the electrical conductivity (EC) and pH. An ammonium acetate method was used for cation exchange capacity (CEC) analyses (Richard, 1954). The pH_{pzc} (point of zero charge) was examined for the pH range of 2.0 to 12 by using 0.1 M NaCl (Ahmad et al., 2019b). The surface morphology of the adsorbents was determined by coating the samples with nanogold particles and then analyzing with a EFI S50 Inspect (Netherlands) scanning electron microscope (SEM). Different magnifications were used to capture images of the samples at 30 kV under high vacuum conditions. The composition of the functional groups was explored with a Bruker Alpha-Eco (Bruker Optics Inc.) ATR-Fourier transforms infrared spectroscopy (FTIR). The mineralogical phases of the adsorbents were determined by analyzing a portion of the adsorbent with a MAXima_X XRD-7000 (Shimadzu, Japan).

2.4. Sorption batch trials

A series of different adsorption batch studies were conducted to test the efficiency of the synthesized adsorbents for removing STZ (Sigma–Aldrich Inc.) antibiotics from aqueous solutions. Initially, STZ was dissolved in 1.0% methanol aqueous solution to prepare a 1000 mg L^{-1} STZ stock solution. The adsorption batch trials were conducted by diluting the stock solution in deionized water and adjusting the required pH. Next, 20 mL of the STZ solution was poured into polypropylene tubes and 10 mg of adsorptive material was added. The suspension was mechanically shaken at 150 rpm for a specified period of time at room temperature (23 °C ± 2 °C). This procedure was repeated three times for every adsorbent and a blank. Next, the suspension was withdrawn from the shaker, filtered through 0.45 µm syringe filters and the remaining STZ concentration was analyzed using high-performance liquid chromatography (Prominence-i, LC-2030C, Shimadzu, Japan) attached with a reversed-phase Raptor C18 column and a PDA detector. The STZ analyses were performed by using a gradient flow comprised of a 70% mobile phase A (99.9% of ultrapure water and 0.1% of formic acid) and a 30% mobile phase B (99.9% of acetonitrile and 0.1% of formic acid) (Ahmed et al., 2017). A flow rate of 0.15 mL min^{-1} with 10 µL of injection volume was used. The STZ adsorption capacity of the adsorptive materials was calculated by using Eq. (1):

$$q_e = \frac{V}{m}(C_o - C_t) \tag{1}$$

where q_e is the adsorbed amount of STZ (mg g^{-1}) at time t, C_o is initial STZ concentration (mg L^{-1}), C_t is the remaining STZ concentration (mg L^{-1}), V is the volume of the STZ solution (L), and m is the dose of adsorbent material (g).

A pH range of 3.0 – 9.0 was used to evaluate the effect of initial solution pH on the removal of STZ from the aqueous media at 100 mg STZ L^{-1}. For the kinetics trials, an initial STZ concentration of 100 mg L^{-1} and a pH of 4.5 were used and the remaining STZ concentrations in the solutions were analyzed after 0.0 to 1440 min. The equilibrium batch studies were performed with dif-

ferent initial STZ concentrations between 0.0 and 100 mg L^{-1} and with an initial solution pH of 4.5.

2.4.1. Kinetics modeling

Kinetic adsorption data was simulated using several kinetic models (Ahmad et al., 2018b). The mathematical expressions of the kinetic models used are shown in Eq. (2) to (6):

$$\text{Pseudo} - \text{first} - \text{order} \quad ln(q_e - q_t) = ln(q_e) - k_1't \tag{2}$$

where, q_e is the adsorption capacity (mg g^{-1}), k'_1 is the rate constant, and t is tim.

$$\text{Pseudo} - \text{second} - \text{order} \quad \frac{t}{Q_t} = \frac{1}{k_2 q_e^2} + \frac{t}{q_e} \tag{3}$$

where, k_2 is the pseudo-second-order rate constant

$$\text{Elovich} \quad Q_t = \frac{1}{\beta}ln(\alpha\beta) + \frac{1}{\beta}lnt \tag{4}$$

where, β = Elovich rate constant, α = initial adsorption rate (mg g^{-1} min^{-1})

$$\text{Intraparticle diffusion} \quad Q_t = c + k_{id}t^{0.5} \tag{5}$$

where, c represents intraparticle diffusion constant, and k_{id} is the apparent diffusion rate constant [(mg g^{-1})$^{0.5}$]

$$\text{Power function} \quad ln(Q_t) = ln(b) + k_f((ln(t)) \tag{6}$$

where, b is the rate constant, and k_f is therate coefficient (mg g^{-1} min^{-1})

2.4.2. Isotherm modeling

The equilibrium adsorption data was simulated by using different isotherm models as shown in Eq. (7) to (11) (Redlich and Peterson, 1959; Ahmad et al., 2018b):

$$\text{Freundlich} \quad q_e = K_F C_e^{1/n} \tag{7}$$

where, K_F is the Freundlich isotherm constant (mg g^{-1})(L mg^{-1})$^{1/n}$, n is the adsorption intensity, and C_e is initial concentration of STZ

$$\text{Langmuir} \quad q_e = \frac{Q_L C_e K_L}{1 + K_L C_e} \tag{8}$$

where, K_L is Langmuir isotherm constant (L mg^{-1}) and Q_L is maximum adsorption capacity (mg g^{-1})

$$\text{Redlich} - \text{Peterson} \quad q_e = \frac{AC_e}{1 + BC_e^g} \tag{9}$$

where, A (L g^{-1}) and B ([L mg^{-1}]^g) are constants

$$\text{Temkin} \quad q_e = \frac{RT}{b}ln(AC_e) \tag{10}$$

where, b represents Temkin isotherm constant, A represents binding constant (L g^{-1}), T is absolute temperature, and R is gas constant.

$$\text{Dubinin} - \text{Radushkevich} \quad q_e = q_D \exp\left(-B_D\left[RTln\left(1 + \frac{1}{C_e}\right)\right]^2\right) \tag{11}$$

where, q_D is maximum adsorption capacity (mg g^{-1}), B_D is isotherm constant (mol^2/kJ^2)

The bonding energy (E) was calculated by using Eq. (12).

Table 1
Chemical and proximate characterization of the produced adsorptive materials (CW: conocarpus tree waste, BC: biochar derived from CW, CBC: chitosan-BC beads, and CBC-Fe: magnetic chitosan-BC beads).

Materials	Yield	EC (dS m^{-1})	pH	pH$_{pzc}$	Moisture (%)	Mobile matter (%)	Ash (%)	Resident material (%)
CW	–	0.89 ± 0.05	6.18 ± 0.88	–	4.96 ± 0.54	82.65 ± 2.65	8.54 ± 0.83	3.85 ± 0.31
BC	34.61 ± 2.82	1.54 ± 0.12	9.31 ± 1.01	7.55 ± 0.53	0.26 ± 0.05	45.84 ± 2.85	21.95 ± 1.18	31.95 ± 2.37
CBC	–	2.83 ± 0.14	8.78 ± 0.98	8.57 ± 0.86	3.32 ± 0.21	40.35 ± 1.75	30.92 ± 2.02	25.40 ± 2.84
CBC-Fe	–	1.03 ± 0.08	6.55 ± 0.72	5.61 ± 0.56	1.40 ± 0.18	30.84 ± 1.89	44.10 ± 3.21	21.66 ± 1.59

$$E = \frac{1}{\sqrt{2B_D}} \qquad (12)$$

3. Results

3.1. Characterization of the adsorptive materials

Table 1 shows the chemical and proximate properties of the materials. The pyrolysis of the CW yielded 34.61% of BC. The EC of the CW increased with the thermalization process in BC, CBC, and CBC-Fe. The CBC had the highest EC value (2.83 dS m^{-1}) than the other materials. Pyrolyzing the CW increased the pH by three units, while treatment with chitosan and chitosan plus Fe decreased the pH by one and three units, respectively. CBC exhibited the highest pH$_{pzc}$ (8.57), followed by BC (7.55) and CBC-Fe (5.61). The results of proximate analyses indicated that the highest

moisture contents were in CW (4.96%), followed by CBC (3.32%), and the lowest moisture contents occurred in CBC-Fe (1.40%), and BC (0.26%). Overall, mobile matter contents were reduced, however, the resident matter and ash contents increased with the pyrolysis process. The highest ash contents were in CBC-Fe (44.10%) compared with BC (21.95%) and CBC (30.92%). Fig. 1 displays the captured SEM images of the adsorptive materials. The surface of the BC is rough and porous, while, deposits of chitosan and iron particles can be seen in the CBC and CBC-Fe. Fig. 2 displays the X-ray diffraction (XRD) patterns of the adsorptive materials before and after STZ adsorption. Fig. 2a displays the XRD patterns of the adsorptive materials before STZ removal. Peaks appearing at 2θ of 26.6°, 35.9°, and 57.7° in CBC-Fe, were designated as iron. The peak appearing at 9.1° in CBC was due to the presence of chitosan. A sharp peak appearing at 14.2° in CW and BC was assumed to be mellite. Similarly, two peaks representing the presence CaCO$_3$ were visible in CW, BC, and CBC at 31.5° and 37.9°, but were absent
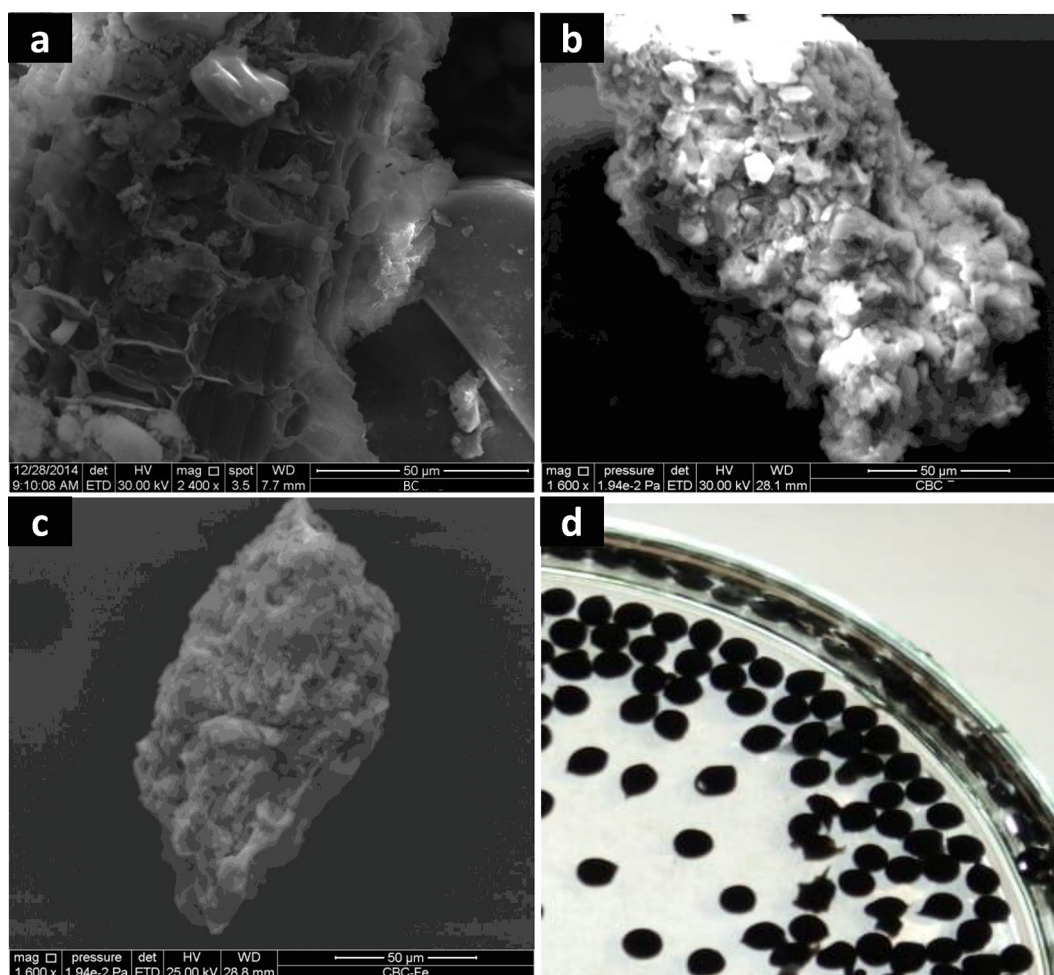
Fig. 1. Scanning electron microscope images of (**a**) conocarpus tree waste derived biochar (BC), (**b**) chitosan-BC beads (CBC), (**c**) magnetic chitosan-BC beads (CBC-Fe), (**d**) and synthesized microspheres.
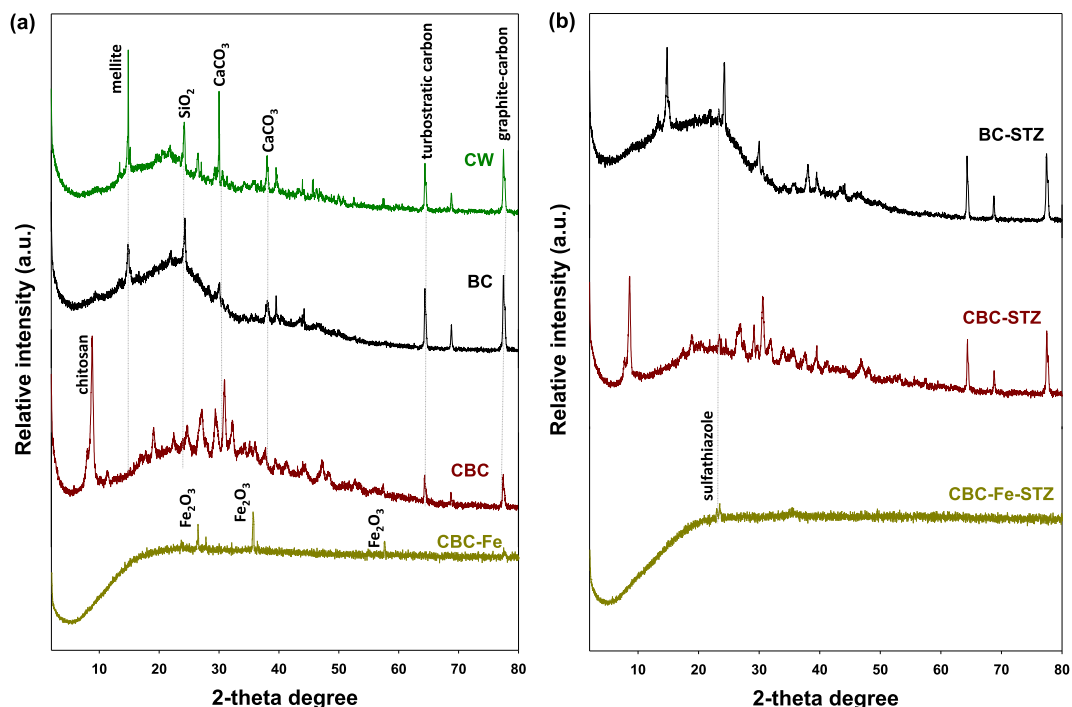
Fig. 2. XRD (X-ray diffraction) patterns of conocarpus tree waste (CW), biochar derived from CW (BC), chitosan-BC beads (CBC), and magnetic chitosan-BC beads (CBC-Fe) before (**a**) and after (**b**) sulfathiazole adsorption.
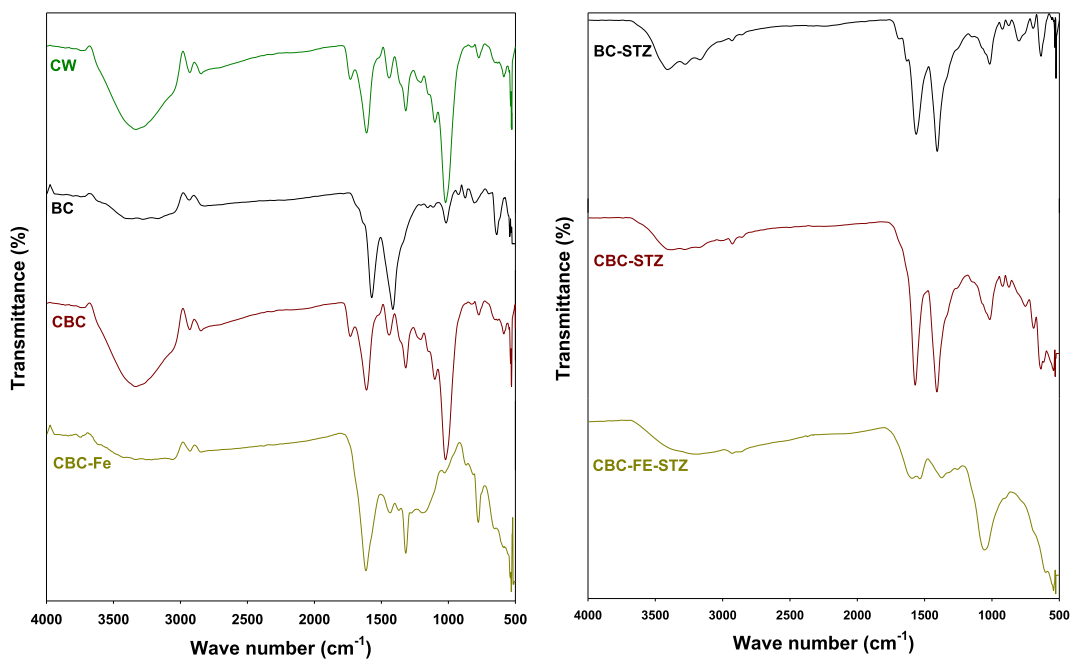
Fig. 3. FTIR (Fourier transform infrared spectroscopy) spectra of conocarpus tree waste (CW), biochar derived from CW (BC), chitosan-BC beads (CBC), and magnetic chitosan-BC beads (CBC-Fe) before (**a**) and after (**b**) sulfathiazole adsorption.

in the CBC-Fe beads. Additional peaks appearing at 2θ of 24.7°, 64.6°, and 77.9° were determined to be SiO_2, turbostratic carbon, and graphite carbon, respectively. The FTIR spectra, as shown in Fig. 3, exhibited a broad absorption band around 3320 cm^{-1}, which was attributed to O–H stretching vibrations of water molecules. In all the adsorptive materials, C = O stretching vibrations associated with carboxyl and carbonyl groups were detected by a band

around 1610 cm^{-1}. An absorbance band around 1050 cm^1 was attributed to C–O–C stretching vibrations in CW. The absorbance bands ranged from 1310 to 1460 cm^{-1} were detected in all of the adsorptive materials. These were attributed to C–H stretching vibrations. Similarly, aliphatic C–H stretching was found in all the materials around 2980 cm^{-1}. The peaks of the Fe–O functional groups occurred around 790 and 1170 cm^{-1}.

3.2. Adsorption studies

3.2.1. Effect of pH on STZ adsorption

The effect of pH on STZ removal by synthesized adsorptive materials was studied in pH range of 3.0 to 9.0. Overall, the highest STZ adsorption was observed at pH 5.0 in all the adsorptive materials, which subsequently decreased with increasing solution pH (Fig. 4a). The adsorption capacity of CBC-Fe at pH 5.0 was 78.21 mg g⁻¹, while the adsorption capacity of CBC and BC at pH 5.0 was 35.33 and 26.74 mg g⁻¹. A sudden drop in STZ adsorption was observed when the pH increased above 6.0 in all the adsorptive materials. Overall, CBC-Fe showed the highest STZ adsorption at all pH levels as compared to rest of the adsorbents. Table 1 shows that BC, CBC, and CBC-Fe contained a pH_{pzc} of 7.55, 8.57, and 5.61, respectively.

3.2.1.1. Kinetic adsorption trials.
Fig. 5a illustrates the dynamics of STZ adsorption onto the synthesized adsorptive materials, which can be broken down into three distinct phases. A relatively quick adsorption phase was observed during initial 90 min, followed by a comparatively slow phase (90 – 180 min), and finally reaching an equilibrium state (360 min and onward). Overall, CBC-Fe showed the highest STZ adsorption capacity compared with the other tested adsorptive materials, suggesting its superior efficacy for STZ removal. To further evaluate the STZ adsorption process, the data was simulated with kinetic models. The estimated standard error of the estimate (*SEE*) values were less than 1.0 for all the simulated kinetic models, indicating good fit between the data and the models (Table 2). Table 2 shows the associated R^2 values, which indicate the best fit with pseudo-second order (R^2 = 0.99) and Elovich (R^2 = 0.90–0.98) kinetic models (Fig. 5b and c, respec-

tively), while, with poorer fit with the intraparticle diffusion and power function (R^2 = 0.75–0.88 and 0.82–0.95, respectively) models (Fig. 5d and e, respectively). Table 3 shows the predicted parameters from the kinetics adsorption models. Predicted STZ adsorption from the pseudo-second order model was highest for CBC-Fe (75.84 mg g⁻¹), followed by CBC (42.73 mg g⁻¹) and BC (34.05 mg g⁻¹). Similarly, CBC-Fe exhibited the highest rate constants as predicted by the pseudo-second order (k^2 = 3.0 × 10⁻⁴), Elovich (β = − 0.338), and power function (b = 1.051) models. Similarly, the predicted pseudo-second order initial sorption constant (α) was highest for CBC-Fe (11.15 mg g⁻¹ min⁻¹) compared with BC and CBC. The highest predicted values of the apparent diffusion rate constant (k_{id}) were for CBC-Fe (4.45 [mg g⁻¹]⁻⁰·⁵), compared to BC (0.881 [mg g⁻¹]⁻⁰·⁵) and CBC (1.129 [mg g⁻¹]⁻⁰·⁵). Overall, CBC-Fe removed the highest amount of STZ from the contaminated water compared to the other adsorbents tested in this study. After 1140 min, CBC-Fe resulted in 83% and 119% higher adsorption than that of CBC and BC, respectively. Fig. 5f shows the highest adsorption enhancement percentage of CBC-Fe as compared to BC and CBC.

3.2.1.2. Equilibrium adsorption trials.
The equilibrium adsorption trials were conducted using different initial STZ concentrations. The data generated from the STZ equilibrium adsorption trials were simulated using various isotherms models (Fig. 6). At lower initial STZ concentrations, an H-type isotherm was constructed by all the adsorptive materials. Contrarily, the shape of the isotherm transformed to L-type at higher initial STZ concentrations. The parameters obtained from the non-linear isotherm models are presented in Table 4. The calculated R^2 values demonstrated that the best fits were obtained from the Langmuir (R^2 = 0.97 – 0.99), Freundlich (R^2 = 0.94 – 0.99), Redlich–Peterson (R^2 = 0.98 – 0.99), and Temkin (R^2 = 0.94 – 0.99) models. The Dubinin-Radushkevich model only resulted in a moderate fit (R^2 = 0.84 – 0.96). The Langmuir model predicted Q_L was the highest for CBC-Fe (98.67 mg g⁻¹), while it was 56.54 mg g⁻¹ for CBC and 48.63 mg g⁻¹ for BC. Similarly, the Dubinin-Radushkevich model predicted Q_D was the highest for CBC-Fe (72.13 mg g⁻¹). Moreover, the K_F values were higher for CBC-Fe (11.24 L g⁻¹) than CBC (3.04 L g⁻¹) and BC (4.36 L g⁻¹). Likewise, b was the highest for CBC-Fe (20.26 J mol⁻¹), compared to CBC (10.89 J mol⁻¹) and BC (7.57 J mol⁻¹). The values of g were less than unity (0.456–0.811) for all the adsorptive materials. Likewise, the values of E were also lower for all the materials tested in this study (less than 8.0 kJ g⁻¹). Additionally, the favorability of STZ adsorption process was further predicted by 1/n values from the Freundlich model. The values of 1/n for all the adsorbents ranged from 0.504 to 0.549. Overall, the STZ adsorption capacity of CBC and CBC-Fe increased by 16.2%–25.6% and 74.5%–108.8%, respectively, as compared to the pristine BC (Fig. 6f).

4. Discussion

The adsorptive materials exhibited varied chemical and proximate characteristics. The variations in pH was due to thermalization and composite formation with Fe and chitosan. The increased EC and pH values in biochar based materials indicated the removal of acidic functional groups and condensation of alkali salts during the pyrolysis process (Usman et al., 2015). However, the lower pH of the CBC-Fe could be due washing out of the soluble salts during several washings performed prior to the beads fabrication. Likewise, the highest ash contents in CBC-Fe were probably due to the existence of thermally stable Fe contents, which may have been confused with the ash contents. The XRD results demonstrated a successful deposition of iron particles onto the biochar
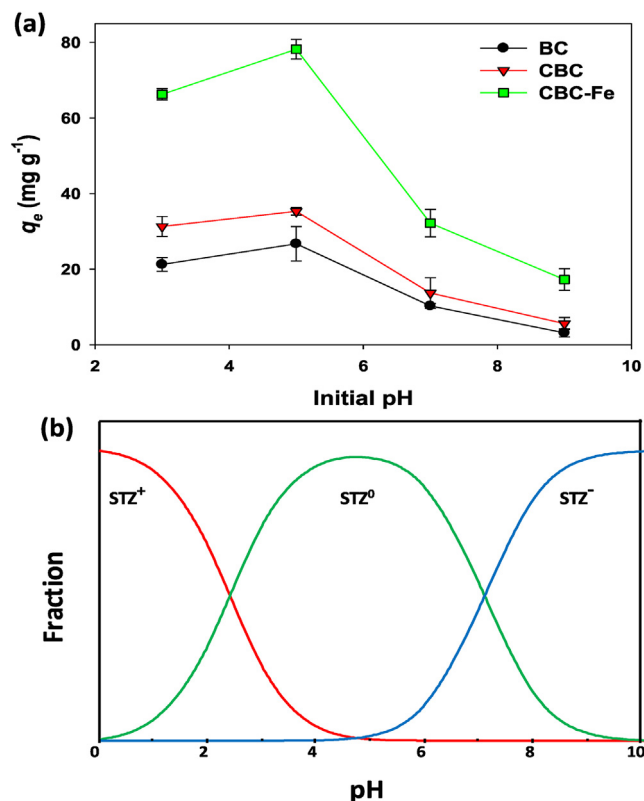
Fig. 4. (**a**) Effect of initial solution pH on sulfathiazole (STZ) adsorption onto conocarpus tree waste derived biochar (BC), chitosan-BC beads (CBC), and magnetic chitosan-BC beads (CBC-Fe), and (**b**) changes in STZ speciation with changing solution pH.
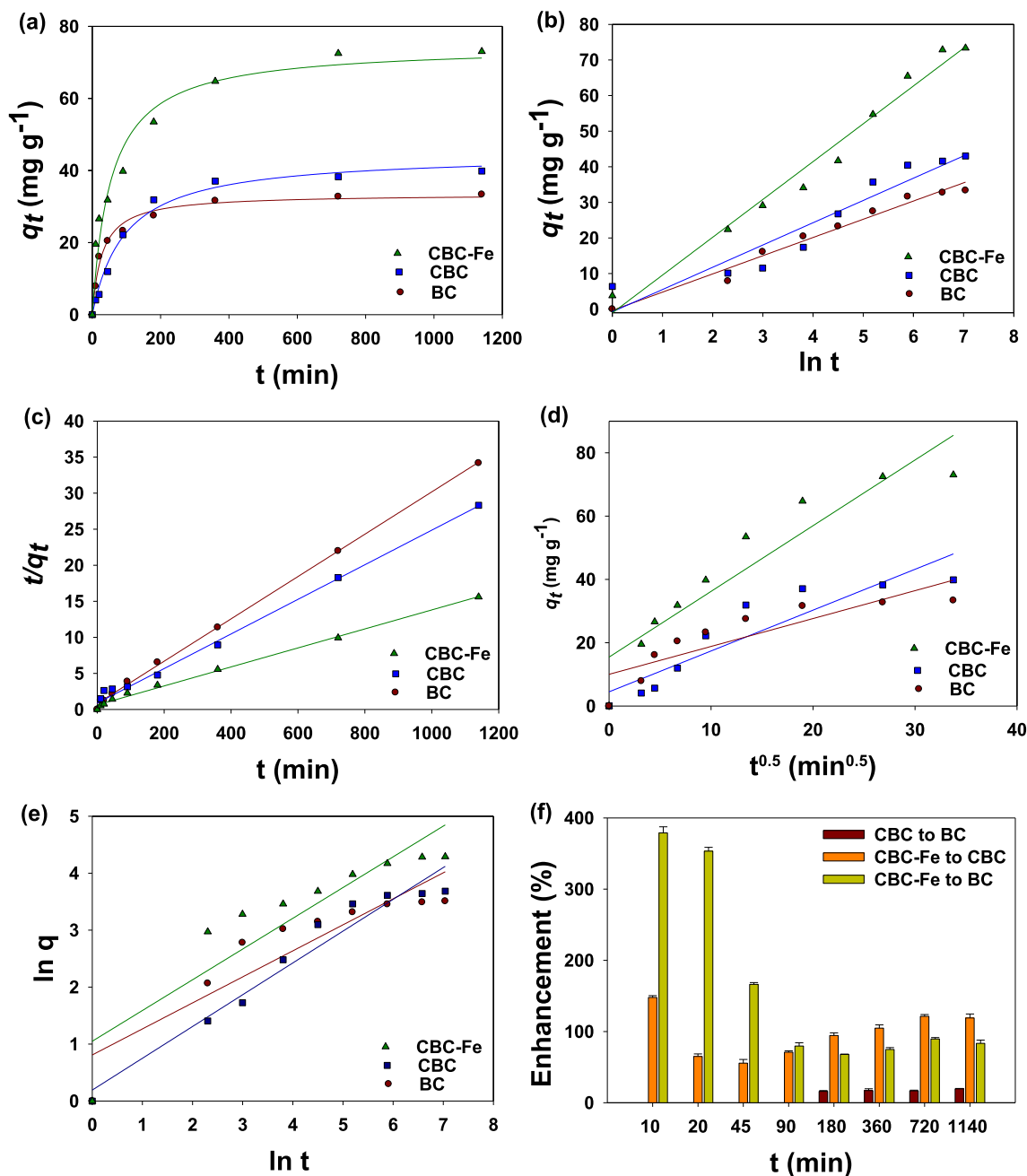
Fig. 5. Sulfathiazole (STZ) adsorption kinetics (**a**) effect of contact time on STZ adsorption, (**b**) Elovich (**c**) pseudo-second order, (**d**) intraparticle diffusion, and (**e**) power function kinetic models by conocarpus tree waste derived biochar (BC), chitosan-BC beads (CBC), and magnetic chitosan-BC beads (CBC-Fe), as well as enhancement in adsorption by modified BCs (**f**) as compared to the other tested adsorbents.

matrix with occurrence of peaks at 26.6°, 35.9°, and 57.7° in CBC-Fe. However, peak appearing at 9.1° in CBC was of chitosan, which was not visible in CBC-Fe due to the deposition of iron particles. It was observed that mellite disappeared in the CBC and CBC-Fe due to composite formation (Ahmad et al., 2019b). The peaks regarding SiO_2, turbostratic carbon, and graphite carbon were seen in the XRD pattern of CW, BC, and CBC, while these were absent in the CBC-Fe beads (Ahmad et al., 2020). The FTIR spectra of the produced adsorptive materials before and after STZ removal were generated for this study. The surface functional groups of adsorptive materials are critical for adsorption efficiency. The FTIR results demonstrated the successful binding of Fe particles to the biochar matrix. Further, the FTIR spectra showed that the beads were successfully synthesized by compositing with biochar, chitosan, and

Fe particles. A broad absorption band of O–H stretching vibrations due to water molecules was larger in CW and CBC, indicating higher moisture contents, while it was smaller in BC and CBC-Fe, showing lower moisture contents. This could also be correlated whith the moisture contents of the materials provided in Table 1. The presence of C–O–C stretching vibrations in CW indicated the occurrence of non-decomposed oxygenated groups. This band was reduced in BC due to the thermalization process, and vanished in CBC-Fe due to deposition of iron particles. It further increased in CBC, which could be due to the mixing of N–H associated with chitosan.

The effectiveness of the produced adsorptive materials for STZ removal from contaminated aqueous media was evaluated through sorption batch experiments. It was seen that the adsorption of STZ

Table 2
Coefficient of determination (R^2) and standard error of estimate (*SEE*) of kinetic models for sulfathiazole adsorption onto conocarpus tree waste derived biochar (BC), chitosan-BC beads (CBC), and magnetic chitosan-BC beads (CBC-Fe).

Adsorbent		BC	CBC	CBC-Fe
First order	R^2	0.51	0.62	0.67
	SEE	0.026	0.017	0.026
Second order	R^2	0.09	0.18	0.16
	SEE	3.1×10^{-3}	0.114	5.8×10^{-3}
Pseudo-first order	R^2	0.71	0.75	0.83
	SEE	0.026	0.017	0.052
Pseudo-second order	R^2	0.99	0.99	0.99
	SEE	0.029	0.003	0.015
Elovich	R^2	0.98	0.90	0.98
	SEE	1.2×10^{-4}	8.1×10^{-5}	5.3×10^{-3}
Intraparticle diffusion	R^2	0.75	0.84	0.88
	SEE	4.8×10^{-4}	7.3×10^{-4}	1.7×10^{-3}
Power function	R^2	0.83	0.95	0.82
	SEE	3.2×10^{-4}	7.0×10^{-4}	2.5×10^{-4}

Table 3
Parameters obtained from the kinetic models for sulfathiazole adsorption onto conocarpus tree waste derived biochar (BC), chitosan-BC beads (CBC), and magnetic chitosan-BC beads (CBC-Fe).

Model	Parameter	Unit	BC	CBC	CBC-Fe
First order	k^1	–	1.4×10^{-3}	2.1×10^{-3}	1.7×10^{-3}
Second order	k^2	–	-2.6×10^{-5}	-8.8×10^{-5}	-1.5×10^{-5}
Pseudo-first order	$k^{1\prime}$	–	-1.4×10^{-3}	-1.5×10^{-3}	-1.5×10^{-3}
	q_e	mg g^{-1}	3.098	3.547	4.058
Pseudo-second order	$k^{2\prime}$	–	1.0×10^{-4}	2.9×10^{-4}	3.0×10^{-4}
	q_e	mg g^{-1}	34.05	42.73	75.84
	h	mg g^{-1} min^{-1}	1.227	0.542	1.612
Elovich	α	mg g^{-1} min^{-1}	5.12	6.8	11.15
	β	–	-5.068	-7.726	-0.338
Intraparticle diffusion	k_{id}	[(mg g^{-1})$^{-0.5}$].	0.881	1.291	4.45
	c	–	4.45	10.00	15.45
Power function	k_f	mg g^{-1} min^{-1}	0.457	0.558	0.584
	b	–	0.808	0.193	1.051

suddenly dropped as solution pH increased above 6.0, indicating the changes in the surface charges of the adsorbent/adsorbate, which can be correlated with pH$_{pzc}$. As the solution pH crosses the pH$_{pzc}$ of each adsorbent, the surface of the materials become negatively charged (Tran et al., 2016). On the other hand, STZ molecules are amphoteric in nature, thus, they are highly susceptible to any change in solution pH (Fig. 4b). Previously, it was reported that the STZ molecule behaves as a neutral ion (STZ^0) at pH 3.0 – 6.0 (Teixidó et al. 2011). However, as pH increases, the STZ molecules become negatively charged (STZ$^-$), and, conversely, become positively charged (STZ$^+$) if the pH decreases below 3.0 (Teixidó et al., 2011). Thus, the solution pH above 6.0 in this study resulted in an anionic form of STZ i.e., STZ$^-$. This anionic form developed electrostatic repulsive interactions with negatively charged surfaces of the adsorptive materials, subsequently reducing the STZ adsorption. However, compared to the rest of the adsorbents, CBC-Fe resulted in higher adsorption capacity, even above pH 7.0. This suggests that CBC-Fe has higher affinity toward STZ molecules. When the pH reached 9.0, affinity was reduced by 4.5-fold for CBC-Fe, 6.3-fold for CBC, and 8.5-fold for BC. The highest STZ adsorption capacity of CBC-Fe could be due to the enhanced surface area, presence of Fe particles, and possible π-donation capacity.

Likewise, the STZ dynamics were studied in kinetics sorption trials. The rate of the adsorption was higher at the beginning, which could be due to the more active sorption sites. As time progressed, the active adsorption sites were slowly occupied until an equilibrium state is reached, with no more active adsorption sites. The sorption data was simulated with the kinetics adsorption models. The results shown that pseudo-second order, Elovich, and power function models were fitted well with the adsorption data,

indicating that STZ had chemically adsorbed to the synthesized adsorptive materials (Wang and Guo, 2020a), which was further augmented by diffusion into the pores (based on results from the intraparticle diffusion model). The higher apparent diffusion rate constant of CBC-Fe indicated a quicker diffusion of STZ molecules into the porous surfaces of the CBC-Fe matrix (Ahmad et al., 2019b). Similarly, CBC-Fe showed higher rate constants, suggesting that less time was required by this adsorbent to remove STZ from contaminated water. Overall, the kinetics adsorption modeling suggested that chemical adsorption, aided by the diffusion of the adsorptive materials into the pores, were responsible for the removal of STZ from contaminated water.

The results of equilibrium adsorption studies showed that the STZ adsorption increased with increasing the initial STZ concentration in the solution (Liu et al., 2018). Therefore, it generated an H-type isotherm at lower initial STZ concentrations due to the abundance of active sorption sites on the adsorbents. Nevertheless, when the initial STZ concentration increases in the solution, the active adsorption sites become occupied by the STZ molecules until an equilibrium state is reached, indicating no further free adsorption sites. Consequently, the shape of the isotherm is transformed into L-type. The equilibrium adsorption data was simulated by the isotherm models. The STZ adsorption data was best described by Langmuir, Freundlich, Redlich–Peterson, and Temkin isotherms, indicating both mono- and multilayer adsorption of STZ onto the synthesized materials (Wang and Guo, 2020b). The Redlich–Peterson model integrates the properties of both the Freundlich and Langmuir models. Thus, for this paper, the best fitness from Redlich–Peterson isotherm suggested the occurrence of multiple mechanisms for STZ adsorption onto the synthesized adsorbents (Liu et al., 2010). However, the lower g values indicated a higher
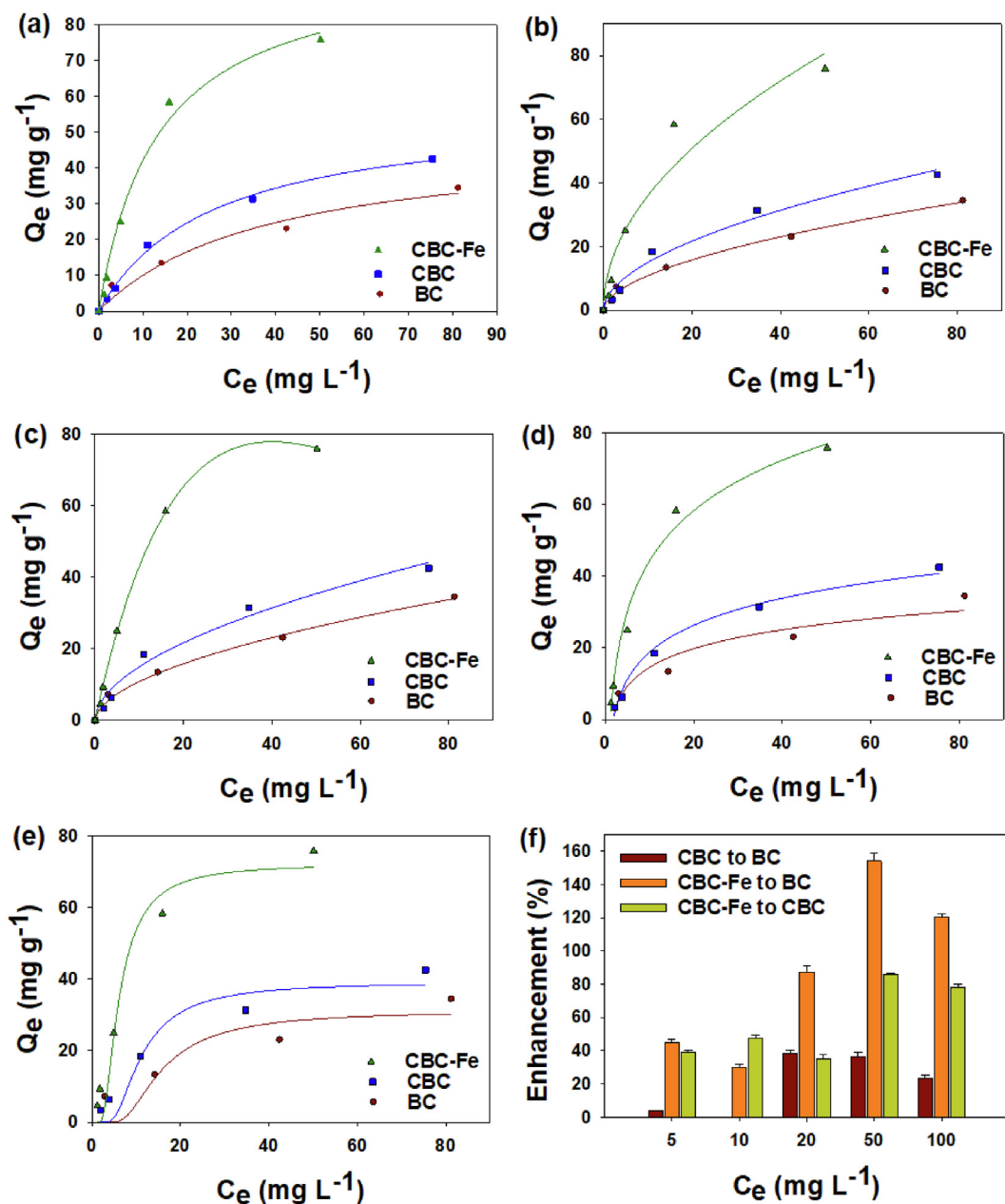
Fig. 6. Sulfathiazole adsorption isotherms of Langmuir (**a**); Freundlich (**b**); Redlich–Peterson (**c**); Temkin (**d**); and Dubinin– Radushkevich (**e**) models by conocarpus tree waste derived biochar (BC), chitosan-BC beads (CBC), and magnetic chitosan-BC beads (CBC-Fe), as well as enhancement in adsorption by modified BCs (**f**) as compared to the other tested adsorbents.

imitation for the Langmuir isotherm. The values of E were less than $8.0 \, kJ \, g^{-1}$, indicating the absence of an ion-exchange phenomena in STZ removal process (Wang and Guo, 2020b; Ahmad et al., 2018b). Overall, CBC-Fe exhibited the highest Q_L, Q_D, K_F, and b, while the lowest E and $1/n$, indicating that it is the most efficient adsorbent for STZ removal from contaminated aqueous media, as compared to the other tested adsorptive materials.

As the characteristics of adsorbate and adsorbent, as well as the adsorption conditions significantly influence the adsorption process, therefore, the mechanisms involved in adsorption process differ by adsorbent type and targeted contaminant. The adsorption of antibiotics onto adsorptive materials may follow multiple mechanisms simultaneously (e.g., electrostatic interactions, H-bonding, and π–π electron-donor–acceptor (EDA) interactions). Generally, ionic species are adsorbed via electrostatic interactions onto the

adsorbents. Hence, due to the ionic form of STZ molecules, electrostatic interactions may play a vital role for its removal from contaminated media. Nevertheless, the ionic form of STZ molecule varies with changing pH of the solution. The cationic form of STZ (STZ^+) is prevalent under strong acidic conditions (pH $\sim$ 3.0) while the anionic form (STZ^-) is prevalent at pH of > 6.0. STZ exists as zwitterions (STZ^0) in the pH range of 3.0–6.0 (Teixidó et al., 2011). These changes in the ionic forms of STZ that accompany changes in the solution pH make it a potent compound to be attracted/repelled via electrostatic interactions. The highest STZ removal was seen at pH 5.0 for all of the adsorptive materials, indicating that electrostatic interactions were not the dominant mechanisms for STZ removal. Moreover, lower STZ adsorption above pH 6.0 may be due to the generation of electrostatic repulsions between STZ^- and the negatively charged surface of the adsorptive

Table 4

Parameters obtained from isotherm modeling for sulfathiazole adsorption onto conocarpus tree waste derived biochar (BC), chitosan-BC beads (CBC), and magnetic chitosan-BC beads (CBC-Fe).

Model	Parameter	Unit	BC	CBC	CBC-Fe
Langmuir	Q_L	mg g^{-1}	48.63	56.54	98.67
	K_L	L g^{-1}	0.026	0.039	0.074
	R^2		0.97	0.99	0.99
Freundlich	K_F	(mg g^{-1}) (L mg^{-1})$^{1/n}$	3.04	4.36	11.24
	$1/n$		0.549	0.536	0.504
	R^2		0.99	0.98	0.94
Redlich–Peterson	A_{RP}	L g^{-1}	7.84	46.44	5.72
	B	[L mg^{-1}]^g	7.641	162.01	0.004
	g		0.456	0.465	0.811
	R^2		0.99	0.98	0.99
Temkin	b	(J mol^{-1})	7.57	10.89	20.26
	A_T	L g^{-1}	0.686	0.562	0.894
	R^2		0.94	0.99	0.99
Dubinin-Radushkevich	Q_D	(mg g^{-1})	31.17	39.14	72.13
	E	(kJ g^{-1})	0.082	0.042	0.013
	R^2		0.84	0.92	0.96

materials (Pei et al., 2014). Thus, the Lewis acid-base effects and π-π EDA interactions may be the dominant removal mechanisms at this pH level (Xiang et al., 2019). Sulfonamide and amino groups present on the surface of STZ molecules potentially react with the O–H groups of the adsorptive materials at pH 5.0 via Lewis acid-base reactions. Additionally, STZ molecules behave as π-electron acceptors under acidic pH due to the existence of N-heteroaromatic rings and lone pairs of electrons; whereas, the carbonaceous surfaces can serve as electron donor–acceptor sites (Liu et al., 2016). Therefore, development of stronger π-π EDA interactions by the transferring electrons from the O–H and C–O–C groups of the adsorptive materials to the amino-group of STZ resulted in higher STZ removal. The significance of π-π EDA interactions in the removal of organic contaminants onto carbonaceous surfaces is well-known (Ye et al., 2017; Afzal et al., 2018). Moreover, O–H groups present on biochar surfaces may adsorb STZ by developing H-bonding with –NH groups of the STZ molecules. The probability of such interactions is higher at basic pH levels (Ahmed et al., 2017). Also, results from the intraparticle diffusion model indicate that the porous structure of biochar helps adsorb the STZ ions into the pores, thus aiding its removal (Jing et al., 2014). Overall, the highest STZ adsorption capacity of CBC-Fe could be related to the magnetic properties, more surface functional groups, and higher surface area compared to the other tested adsorbents. Furthermore, the stronger binding of Fe particles with the amino groups of chitosan reduced the precipitation of Fe and resulted in the formation of stable microspheres in CBC-Fe. The transfer of electrons in CBC-Fe was higher due to more conductivity of the magnetic microsphere beads, consequently resulting in stronger π-π EDA interactions (Li et al., 2020). Additionally, the degradation of STZ molecules through CBC-Fe also resulted in higher adsorption capacity (Xu et al., 2012). Free HO• radicals produced from iron ions were captured by the STZ molecules, which subsequently resulted in the degradation of STZ.

XRD and FTIR analyses of the STZ-loaded adsorptive materials were used to further evaluate the STZ adsorption process. A new peak appeared at 23.3° in the XRD pattern for all the adsorptive materials after adsorption was due to the presence of STZ molecules (Fig. 2b). Moreover, Fe$_2$O$_3$ peaks that appeared at 35.9° and 57.7° in CBC-Fe subsequently disappeared after STZ adsorption. Similarly, peak shifts and changes in intensities were observed for the other adsorbents. Variation in band intensities and changes in their appearances suggested interactions of STZ molecules with surface functional groups of the synthesized adsorbent materials (Fig. 3b). The bands representing the Fe–O functional groups around 790 and 1170 cm^{-1}, as well as the C = O bands around 1610 cm^{-1} in CBC-Fe disappeared after STZ adsorption. Similarly,

after STZ adsorption, the C–H bands around 1310 to 1460 cm^{-1} decreased in CBC-Fe, but, increased in BC and CBC. These results indicated successful loading of STZ onto the synthesized adsorptive materials. Hence, it was suggested that π-π EDA interactions and Lewis acid-base reactions were the dominant mechanisms for STZ removal from contaminated water for all the adsorbents tested in this study. Further, diffusion into the pores and H-bonding aided the adsorption of STZ through the synthesized adsorbents, while, degradation of STZ molecules occurred in CBC-Fe resulting in the higher STZ removal.

5. Conclusion

Conocarpus (*Conocarpus erectus* L.) tree waste (CW) derived biochar (BC) was used to fabricate chitosan-BC (CBC) and magnetic CBC (CBC-Fe) microsphere beads. The produced adsorbents were evaluated to assess their efficacy for removal of sulfathiazole (STZ) from aqueous solutions via pH, kinetics, and equilibrium batch type studies. A pH level of 5.0 was found to be optimum for the highest STZ removal. The adsorption data was simulated by kinetics and isotherm models to understand the adsorption process. The maximum adsorption capacity was exhibited by CBC-Fe (98.67 mg g^{-1}), followed by CBC (56.54 mg g^{-1}) and BC (48.63 mg g^{-1}). Similarly, CBC-Fe exhibited the highest rate constant predicted by pseudo-second order, Elovich, and power function models, as well as the highest apparent diffusion rate constant. Overall, STZ adsorption capacities of CBC-Fe and CBC were 74.5%–108.8% and 16.2%–25.6% higher, respectively, compared to the pristine BC. Post STZ adsorption analyses and simulations of kinetics and isotherm models suggested that π-π electron-donor–acceptor interactions and Lewis acid-base reactions were the dominant mechanisms for STZ removal, whereas, intraparticle diffusion and H-bonding further aided the adsorption process. The highest STZ adsorption of CBC-Fe was due to magnetic properties, stronger microsphere beads formation, and generation of HO• radicals. Hence, converting pristine biochar into magnetic chitosan-biochar beads can be implemented as a cost-effective, efficient, and environment friendly approach for STZ removal from contaminated media.

Declaration of Competing Interest

The authors declare that they have no known competing financial interests or personal relationships that could have appeared to influence the work reported in this paper.

Acknowledgement

References

Afzal, M.Z., Sun, X.F., Liu, J., Song, C., Wang, S.G., Javed, A., 2018. Enhancement of ciprofloxacin sorption on chitosan/biochar hydrogel beads. Sci. Total. Environ. 639, 560–569. https://doi.org/10.1016/j.scitotenv.2018.05.129.

Ahmad, M., Ahmad, M., Usman, A.R., Al-Faraj, A.S., Abduljabbar, A., Ok, Y.S., Al-Wabel, M.I., 2019a. Date palm waste-derived biochar composites with silica and zeolite: synthesis, characterization and implication for carbon stability and recalcitrant potential. Environ. Geochem. Health. 41, 1687–1704. https://doi.org/10.1007/s10653-017-9947-0.

Ahmad, M., Ahmad, M., Usman, A.R.A., Al-Faraj, A.S., Abduljabbar, A.S., Al-Wabel, M.I., 2018a. Biochar composites with nano zerovalent iron and eggshell powder for nitrate removal from aqueous solution with coexisting chloride ions. Environ. Sci. Pollut. Res. 25, 25757–25771. https://doi.org/10.1007/s11356-017-0125-9.

Ahmad, M., Ahmad, M., Usman, A.R.A., Al-Faraj, A.S., Ok, Y.S., Hussain, Q., Abduljabbar, A.S., Al-Wabel, M.I., 2018b. An efficient phosphorus scavenging from aqueous solution using magnesiothermally modified bio-calcite. Environ. Technol. 39, 1638–1649. https://doi.org/10.1080/09593330.2017.1335349.

Ahmad, M., Akanji, M.A., Usman, A.R.A., Al-Farraj, A.S.F., Tsang, Y.F., Al-Wabel, M.I., 2020. Turning date palm waste into carbon nanodots and nano zerovalent iron composites for excellent removal of methylthioninium chloride from water. Sci. Rep. 10, 16125. https://doi.org/10.1038/s41598-020-73097-x.

Ahmad, M., Usman, A.R.A., Rafique, M.I., Al-Wabel, M.I., 2019b. Engineered biochar composites with zeolite, silica, and nano-zerovalent iron for the efficient scavenging of chlortetracycline from aqueous solutions. Environ. Sci. Pollut. Res. 26, 15136–15152. https://doi.org/10.1007/s11356-019-04850-7.

Ahmed, M.B., Zhou, J.L., Ngo, H.H., Guo, W., Johir, M.A.H., Sornalingam, K., 2017. Single and competitive sorption properties and mechanism of functionalized biochar for removing sulfonamide antibiotics from water. Chem. Eng. J. 311, 348–358. https://doi.org/10.1016/j.cej.2016.11.106.

Al-Mogbel, M.S., Elabbasy, M.T., Menezes, G.A., Afaq, S., Khan, M., 2015. A brief review on prevalence of antimicrobial residues and antimicrobial resistant bacteria isolated from food in Saudi Arabia. Life Sci. J. 12, 10–15.

Al-Nazawi, M.H., 2006. Resistance and residues of antibacterial in dairy farm and dairy production in al-Hassa region. Saudi Arabia. J. Med. Sci. 6, 202. https://doi.org/10.3923/jms.2006.198.202.

American Society for Testing and Materials (ASTM)., 1989. Standard methods for chemical analysis of wood charcoal, ASTM D1762-84. Philadelphia, PA, USA.

Awad, Y.M., Kim, S.C., Abd, El-Azeem, S.A.M., Kim, K.H., Kim, K.R., Kim, K., Jeon, C., Lee, S.S., Ok, Y.S., 2014. Veterinary antibiotics contamination in water, sediment, and soil near a swine manure composting facility. Environ. Earth. Sci. 71, 1433-1440. https://doi.org/10.1007/s12665-013-2548-z.

Bajpai, S.K., Bajpai, M., Rai, N., 2012. Sorptive removal of ciprofloxacin hydrochloride from simulated wastewater using sawdust: kinetic study and effect of pH. Water Sa 38, 673–682. https://doi.org/10.4314/wsa.v38i5.4.

Boxall, A.B., Kolpin, D.W., Halling-Sørensen, B., Tolls, J., 2003. Peer reviewed: are veterinary medicines causing environmental risks. Environ. Sci. Technol. 37, 286A–294A. https://doi.org/10.1021/es032519b.

Chen, A., Shang, C., Shao, J., Lin, Y., Luo, S., Zhang, J., Huang, H., Lei, M., Zeng, Q., 2017. Carbon disulfide-modified magnetic ion-imprinted chitosan-Fe(III): a novel adsorbent for simultaneous removal of tetracycline and cadmium. Carbohydr. Polym. 155, 19–27. https://doi.org/10.1016/j.carbpol.2016.08.038.

Chen, Y., Shi, J., Du, Q., Zhang, H., Cui, Y., 2019. Antibiotic removal by agricultural waste biochars with different forms of iron oxide. RSC Adv. 9, 14143–14153. https://doi.org/10.1039/C9RA01271K.

Choi, K., Kim, Y., Park, J., Park, C.K., Kim, M.Y., Kim, H.S., Kim, P., 2008. Seasonal variations of several pharmaceutical residues in surface water and sewage treatment plants of Han River. Korea. Sci. Total. Environ. 405, 120–128. https://doi.org/10.1016/j.scitotenv.2008.06.038.

El-Shafey, E.S.I., Al-Lawati, H., Al-Sumri, A.S., 2012. Ciprofloxacin adsorption from aqueous solution onto chemically prepared carbon from date palm leaflets. J. Environ. Sci. 24, 1579–1586. https://doi.org/10.1016/S1001-0742(11)60949-2.

Huang, C.H., Renew, J.E., Smeby, K.L., Pinkston, K., Sedlak, D.L., 2011. Assessment of potential antibiotic contaminants in water and preliminary occurrence analysis. J. Contemp. Water Res. Educ. 120, 4. https://doi.org/10.1142/9789812799555_0004.

Jing, X.R., Wang, Y.Y., Liu, W.J., Wang, Y.K., Jiang, H., 2014. Enhanced adsorption performance of tetracycline in aqueous solutions by methanol-modified biochar. Chem. Eng. J. 248, 168–174. https://doi.org/10.1016/j.cej.2014.03.006.

Kim, S.C., Carlson, K., 2007. Quantification of human and veterinary antibiotics in water and sediment using SPE/LC/MS/MS. Anal. Bioanal. Chem. 387, 1301–1315. https://doi.org/10.1007/s00216-006-0613-0.

Lehmann, J., 2007. Bio-energy in the black. Front. Ecol. Environ. 5, 381–387. https://doi.org/10.1890/1540-9295(2007)5[381:BITB]2.0.CO;2.

Li, X., Cui, K., Guo, Z., Yang, T., Cao, Y., Xiang, Y., Chen, H., Xi, M., 2020. Heterogeneous Fenton-like degradation of tetracyclines using porous magnetic chitosan microspheres as an efficient catalyst compared with two preparation methods. Chem. Eng. J. 379,. https://doi.org/10.1016/j.cej.2019.122324 122324.

Liu, F.F., Zhao, J., Wang, S., Xing, B., 2016. Adsorption of sulfonamides on reduced graphene oxides as affected by pH and dissolved organic matter. Environ. Pollut. 210, 85–93. https://doi.org/10.1016/j.envpol.2015.11.053.

Liu, Q.S., Zheng, T., Wang, P., Jiang, J.P., Li, N., 2010. Adsorption isotherm, kinetic and mechanism studies of some substituted phenols on activated carbon fibers. Chem. Eng. J. 157, 348–356. https://doi.org/10.1016/j.cej.2009.11.013.

Liu, S., Pan, M., Feng, Z., Qin, Y., Wang, Y., Tan, L., Sun, T., 2020. Ultra-high adsorption of tetracycline antibiotics on garlic skin-derived porous biomass carbon with high surface area. New J. Chem. 44, 1097–1106. https://doi.org/10.1039/C9NJ05396D.

Liu, Z., Tian, D., Hu, J., Shen, F., Long, L., Zhang, Y., Yang, G., Zeng, Y., Zhang, J., He, J., Deng, S., Hu, Y., 2018. Functionalizing bottom ash from biomass power plant for removing methylene blue from aqueous solution. Sci. Total Environ. 634, 760–768. https://doi.org/10.1016/j.scitotenv.2018.04.010.

Mututuvari, T.M., Tran, C.D., 2014. Synergistic adsorption of heavy metal ions and organic pollutants by supramolecular polysaccharide composite materials from cellulose, chitosan and crown ether. J. Hazard. Mater. 264, 449–459. https://doi.org/10.1016/j.jhazmat.2013.11.007.

Pei, Z., Yang, S., Li, L., Li, C., Zhang, S., Shan, X.Q., Wen, B., Guo, B., 2014. Effects of copper and aluminum on the adsorption of sulfathiazole and Tylosin on peat and soil. Environ. Pollut. 184, 579–585. https://doi.org/10.1016/j.envpol.2013.09.038.

Peng, L., Ren, Y., Gu, J., Qin, P., Zeng, Q., Shao, J., Lei, M., Chai, L., 2014. Iron improving bio-char derived from microalgae on removal of tetracycline from aqueous system. Environ. Sci. Pollut. Res. 21, 7631–7640. https://doi.org/10.1007/s11356-014-2677-2.

Rafique, M.I., Usman, A.R.A., Ahmad, M., Sallam, A., Al-Wabel, M.I., 2020. In situ immobilization of Cr and its availability to maize plants in tannery waste–contaminated soil: effects of biochar feedstock and pyrolysis temperature. J. Soils Sediments 20, 330–339. https://doi.org/10.1007/s11368-019-02399-z.

Redlich, O.J.D.L., Peterson, D.L., 1959. A useful adsorption isotherm. J. Phys. Chem. 63, 1024-. https://doi.org/10.1021/j150576a611.

Richard, L.A., 1954. Diagnosis and improvement of saline and alkali soils. U.S.D.A. Handbook NO. 60. Oxford and I.B.H. Calcutta.

Teixidó, M., Pignatello, J.J., Beltrán, J.L., Granados, M., Peccia, J., 2011. Speciation of the ionizable antibiotic sulfamethazine on black carbon (biochar). Environ. Sci. Technol. 45, 10020–10027. https://doi.org/10.1021/es202487h.

Tran, H.N., You, S.J., Chao, H.P., 2016. Effect of pyrolysis temperatures and times on the adsorption of cadmium onto orange peel derived biochar. Waste Manag. Res. 34, 129–138. https://doi.org/10.1177/0734242X15615698.

Usman, A.R.A., Abduljabbar, A., Vithanage, M., Ok, Y.S., Ahmad, M., Ahmad, M., Elfaki, J., Sallam, S.A., Al-Wabel, M.I., 2015. Biochar production from date palm waste: charring temperature induced changes in composition and surface chemistry. J. Anal. Appl. Pyrol. 115, 392–400. https://doi.org/10.1016/j.jaap.2015.08.016.

Van Boeckel, T.P., Brower, C., Gilbert, M., Grenfell, B.T., Levin, S.A., Robinson, T.P., Teillant, A., Laxminarayan, R., 2015. Global trends in antimicrobial use in food animals. Proc. Natl. Acad. Sci. USA 112, 5649–5654. https://doi.org/10.1073/pnas.1503141112.

Wang, J., Guo, X., 2020a. Adsorption kinetic models: physical meanings, applications, and solving methods. J. Hazard. Mater. 390,. https://doi.org/10.1016/j.chemosphere.2020.127279 122156.

Wang, J., Guo, X., 2020b. Adsorption isotherm models: Classification, physical meaning, application and solving method. Chemosphere. https://doi.org/10.1016/j.chemosphere.2020.127279 127279.

Wang, J., Wang, S., 2018. Microbial degradation of sulfamethoxazole in the environment. Appl. Microbiol. Biotechnol. 102, 3573–3582. https://doi.org/10.1007/s00253-018-8845-4.

Wang, J., Wang, S., 2019. Preparation, modification and environmental application of biochar: a review. J. Clean. Prod. 227, 1002–1022. https://doi.org/10.1016/j.jclepro.2019.04.282.

Wang, J., Zhuan, R., 2020. Degradation of antibiotics by advanced oxidation processes: An overview. Sci. Total Environ. 701,. https://doi.org/10.1016/j.scitotenv.2019.135023 135023.

Wang, J., Zhuang, S., 2017. Removal of various pollutants from water and wastewater by modified chitosan adsorbents. Crit. Rev. Environ. Sci. Technol. 47, 2331–2386. https://doi.org/10.1080/10643389.2017.1421845.

Wang, J., Chen, X., 2020. Removal of antibiotic resistance genes (ARGs) in various wastewater treatment processes: An overview. Crit. Rev. Environ. Sci. Technol., 1–60 https://doi.org/10.1080/10643389.2020.1835124.

Wang, J., Chu, L., Wojnárovits, L., Takács, E., 2020. Occurrence and fate of antibiotics, antibiotic resistant genes (ARGs) and antibiotic resistant bacteria (ARB) in municipal wastewater treatment plant: An overview. Sci. Total Environ. https://doi.org/10.1016/j.scitotenv.2020.140997 140997.

Wang, J., Zhuan, R., Chu, L., 2019. The occurrence, distribution and degradation of antibiotics by ionizing radiation: an overview. Sci. Total Environ. 646, 1385–1397. https://doi.org/10.1016/j.scitotenv.2018.07.415.

Xiang, Y., Xu, Z., Wei, Y., Zhou, Y., Yang, X., Yang, Y., Yang, J., Zhang, J., Luo, L., Zhou, Z., 2019. Carbon-based materials as adsorbent for antibiotics removal: mechanisms and influencing factors. J. Environ. Manag. 237, 128–138. https://doi.org/10.1016/j.jenvman.2019.02.068.

Xu, L., Wang, J., 2012. Magnetic nanoscaled Fe_3O_4/CeO_2 composite as an efficient Fenton-like heterogeneous catalyst for degradation of 4-chlorophenol. Environ. Sci. Technol. 46, 10145–10153. https://doi.org/10.1021/es300303f.

Yao, Y., Gao, B., Chen, J., Yang, L., 2013. Engineered biochar reclaiming phosphate from aqueous solutions: mechanisms and potential application as a slow-release fertilizer. Environ. Sci. Technol. 47, 8700–8708. https://doi.org/10.1021/es4012977.

Ye, S., Zeng, G., Wu, H., Zhang, C., Liang, J., Dai, J., Liu, Z., Xiong, W., Wan, J., Xu, P., Cheng, M., 2017. Co-occurrence and interactions of pollutants, and their impacts on soil remediation—a review. Crit. Rev. Environ. Sci. Technol. 47, 1528–1553. https://doi.org/10.1080/10643389.2017.1386951.

Yu, Y., Wang, W., Shi, J., Zhu, S., Yan, Y., 2017. Enhanced levofloxacin removal from water using zirconium (IV) loaded corn bracts. Environ. Sci. Pollut. Res. 24, 10685–10694. https://doi.org/10.1007/s11356-017-8700-7.

Zheng, H., Wang, Z., Zhao, J., Herbert, S., Xing, B., 2013. Sorption of antibiotic sulfamethoxazole varies with biochars produced at different temperatures. Environ. Pollut. 181, 60–67. https://doi.org/10.1016/j.envpol.2013.05.056.